Figure 1. Effects of MSCs in the AOM/DSS colitis-associated carcinoma model

AOM/DSS model rats (n = 39) were classified into three groups (n = 13 each group) according to the timing of MSC administration in carcinogenetic phases: MSC untreated control [MSC (-)], tumor initiation (day 0; 'MSC Day0'), and tumor promotion phases (day 9; 'MSC Day9'), as shown in panel A. Brown, orange, and blue bars represent data obtained from MSC (-), MSC Day0, and MSC Day9 groups, respectively. The upper panel of B shows the average tumor number per rat (a total of 271 tumors developed), and the lower panel indicates the average tumor size. *, $P = 0.023$; **, $P = 0.008$. The upper row of the panel C shows that β-catenin protein expression (n = 70 tumor tissues) was regarded as positive when the band intensity was stronger than that in the normal colon in western blot analyses. Twenty-three of 29 (79.3%), 23 of 25 (92.0%), and 13 of 16 (81.2%) tumors examined were positive for β-catenin expression in MSC (-), MSC Day0, and MSC Day9 groups, respectively. The lower row indicates positivity of phospho-β-catenin at Ser33/37/Thr41 in western blot analyses in the three groups. The contingency table analysis reached statistical significance (*$P = 0.0006$). The WNT signal pathway PCR array of representative samples pairs obtained from MSC (-) and MSC Day0 groups was depicted in panel D. PCR and western blot analyses were performed in triplicate unless specified otherwise.

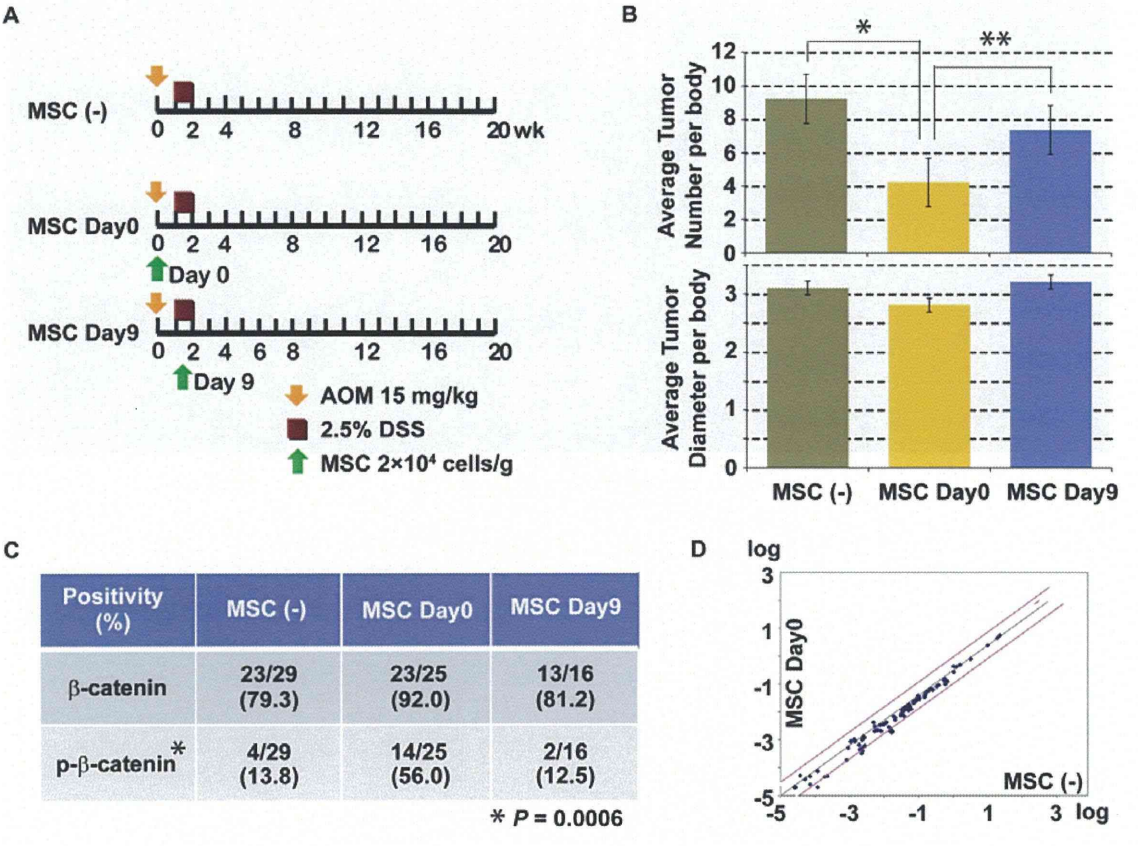

Positivity (%)	MSC (-)	MSC Day0	MSC Day9
β-catenin	23/29 (79.3)	23/25 (92.0)	13/16 (81.2)
p-β-catenin*	4/29 (13.8)	14/25 (56.0)	2/16 (12.5)

* $P = 0.0006$

Figure 2. Double immunofluorescence staining of Smad2 and β-catenin

From the left to right, panels show nuclear counterstaining with DAPI [1], visualization of Smad2 [2] and β-catenin [3] using Alexa Fluor® 488- and 594-labeled secondary antibodies, respectively, and merged images [4]. Panel A shows normal colonic tissues of AOM-untreated healthy rats, panel B shows tumor tissues from the MSC (-) group, and panel C shows tumor tissues from the MSC Day0 group. White arrowheads in panel B indicate nuclear staining of Smad2. Bar scales at the right lower corner in each panel indicated 10 μm.

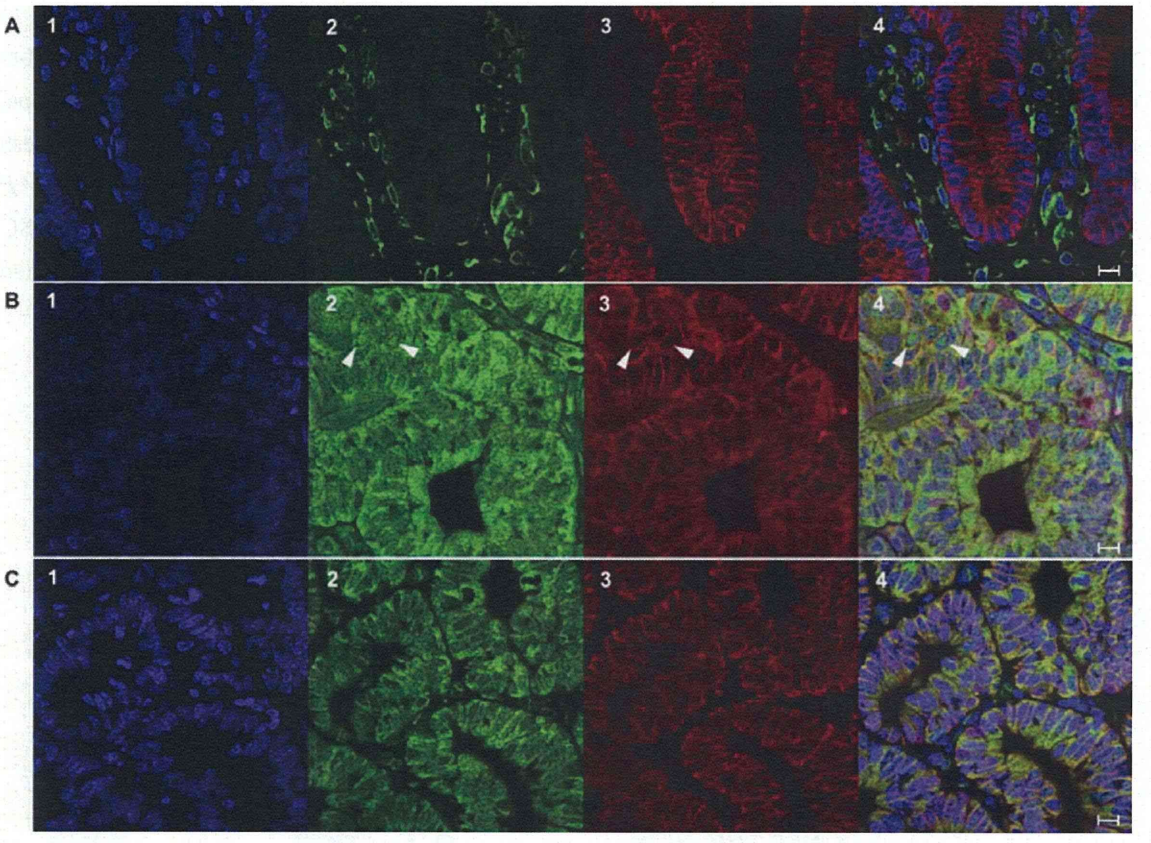

Figure 3. Analysis of the ACF model

ACF model rats (n = 15) were classified into three groups (n = 5 each group) according to the timing of MSC administration either before or after administration of two separate of AOM on Days 0 and 7: MSC (-), MSC pre-AOM (Day–1), and MSC post-AOM (Day 8) groups (A). A total of 400 ACF developed: 213, 95, and 92 in MSC (-), MSC Day–1, and MSC Day8 groups, respectively. The average ACF density is shown in panel B. *1, $P = 4.7E\text{-}4$; *2, $P = 0.001$. The average ACF density in the proximal, middle, and distal colon is shown in panel C. *1, $P = 0.02$; *2, $P = 1.6E\text{-}4$; *3, $P = 0.037$; *4, $P = 0.017$; *5, $P = 0.022$; *6, $P = 0.002$; *7, $P = 0.004$; *8, $P = 4.0E\text{-}5$; *9, $P = 2.2E\text{-}4$; *10, $P = 2.1E\text{-}7$; *11, $P = 1.9E\text{-}6$. Representative ACs, one to more than four ACs per focus, are shown in panels D1–4, respectively. Scale bars: 50 μm. The average density of ACs per focus, one to more than four ACs, is shown in panel E. *1, $P = 0.009$; *2, $P = 0.011$; *3, $P = 5.2E\text{-}5$; *4, $P = 7.3E\text{-}5$; *5, $P = 0.005$; *6, $P = 7.3E\text{-}5$; *7, $P = 5.3E\text{-}5$; *8, $P = 1.7E\text{-}4$; *9, $P = 7.9E\text{-}5$; *10, $P = 0.021$; *11, $P = 0.005$; *12, $P = 4.0E\text{-}6$; *13, $P = 6.4E\text{-}6$; *14, $P = 0.001$; *15, $P = 0.001$. Panel F shows the analysis of TGF-β signaling by western blotting of Smad2 and phospho-Smad2. Lanes 1–5, 6–10, and 11–15 show data for MSC (-) control MSC Day–1, and MSC Day8 groups, respectively.

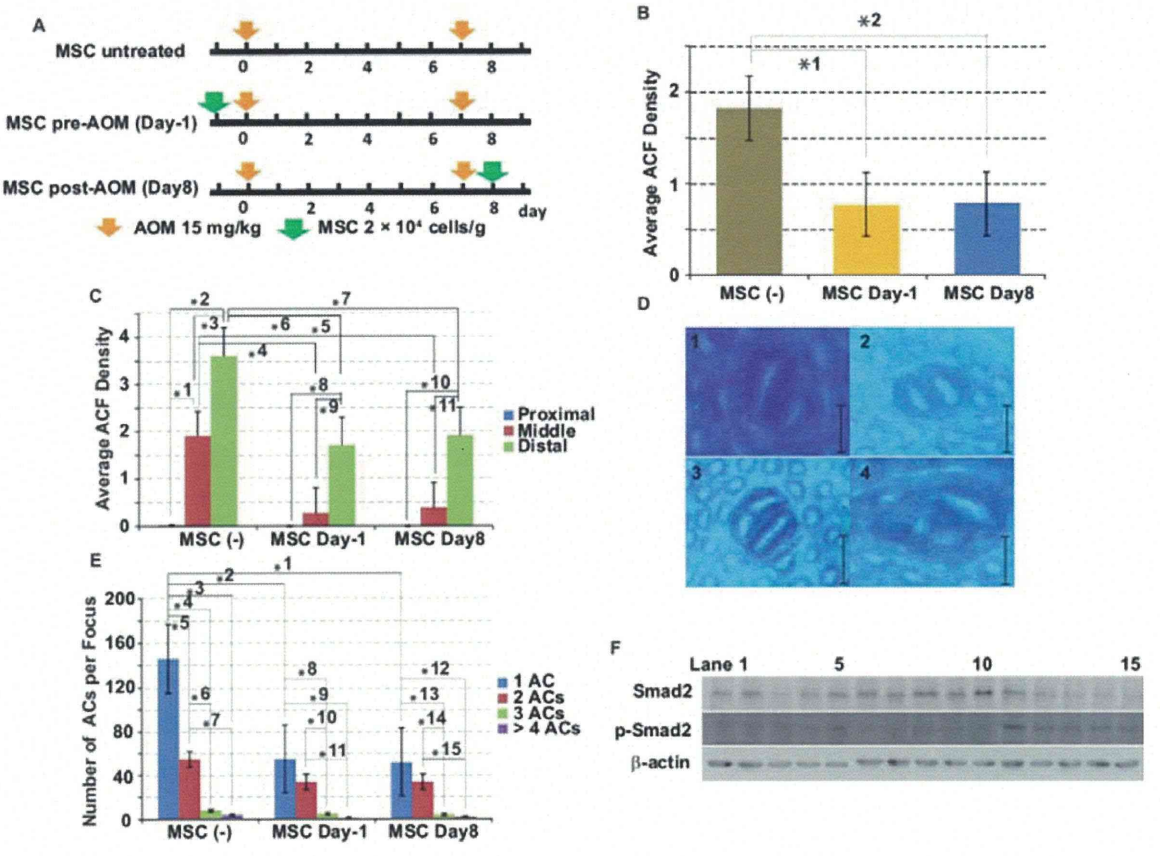

Figure 4. Effects of MSCs on the AARGC

AARGC model rats (n = 15) were classified into five groups (n = 5 each group) according to the treatment at 24 h before administration of a single dose of AOM on Day 0: MSC (-) control (PBS), MSC, HSC, 3Y1, and MSC-CM groups. Rats were sacrificed at 0 h when AOM was intraperitoneally injected at 4, 8, 16, 24, and 48 h for subsequent analyses (A). Representative TUNEL immunostaining is shown for control (upper) and MSC-24h groups (lower) at 8 h. The right panel shows magnified views corresponding to the rectangles in the left panel (B). Bar scales at the right lower corner in each panel indicated 250 μm. The apoptotic index was calculated as the percentage of positive nuclear immunostaining of TUNEL reactions in approximately 1,000 crypt epithelial cells at each indicated time point (C). *MSC *vs.* control, $P = 0.006$; MSC *vs.* HSC, $P =$ 2.9E-4; MSC *vs.* 3Y1, $P = 0.001$; MSC *vs.* MSC-CM, $P =$ 1.7E-4: **MSC *vs.* HSC, $P = 0.010$; MSC *vs.* 3Y1, $P = 0.005$; MSC *vs.* MSC-CM $P =$ 1.3E-5. Representative Ki-67 immunofluorescence in shown for control (left) and MSC groups (right) at 4 h (D). Bar scales at the right lower corner in each panel indicated 10 μm. The Ki-67 labeling index was calculated as the percentage of positive nuclear immunofluorescence in approximately 1,000 epithelial cells at each indicated time point (E). *MSC *vs.* control, $P = 0.037$: **MSC *vs.* control, $P =$ 2.2E-4; MSC *vs.* HSC, $P =$ 3.2E-5; MSC *vs.* 3Y1, $P =$ 0.002. Ki-67 immunofluorescence and TUNEL reactions were performed using at least five different specimens in triplicate. Western blot analyses of Akt and MAP kinase signaling between MSC-treated and MSC-untreated control groups was performed (F).

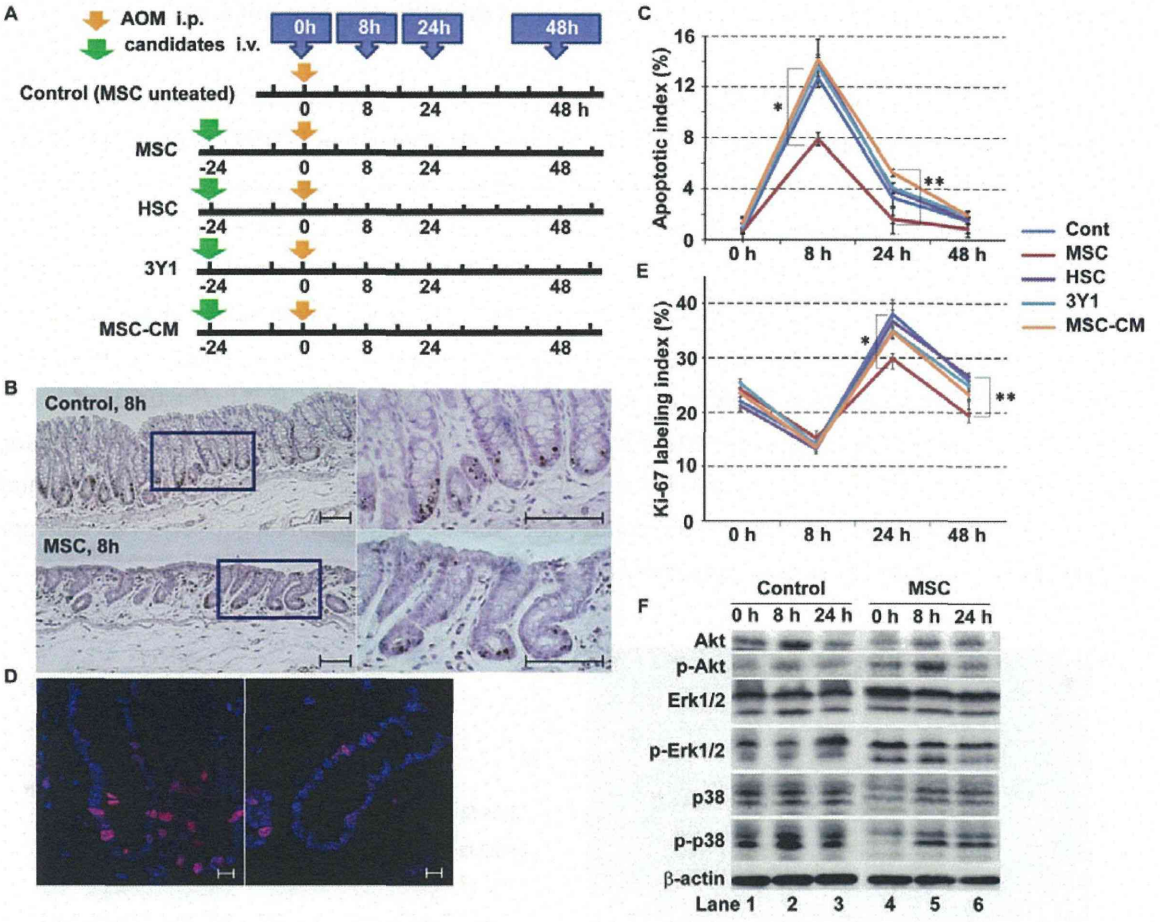
A
AOM i.p.
candidates i.v.
0h
8h
24h
48h
Control (MSC unteated)
MSC
HSC
3Y1
MSC-CM
-24
0
8
24
48 h
B
Control, 8h
MSC, 8h
C
Apoptotic index (%)
0 h
8 h
24 h
48 h
Cont
MSC
HSC
3Y1
MSC-CM
D
E
Ki-67 labeling index (%)
F
Control
MSC
Akt
p-Akt
Erk1/2
p-Erk1/2
p38
p-p38
β-actin
Lane 1 2 3 4 5 6

Figure 5. Mechanistic insight into the suppression of AOM-induced tumor initiation *in vivo*

The results of the *in vivo* immunofluorescence analysis of O^6MeG are depicted in panels A–C. The left panels show nuclei stained with DAPI, the middle panels visualize O^6MeG adducts in nuclear DNA using an Alexa Fluor® 594-labeled secondary antibody, and the right panels are merged images of the left and middle panels in the same row. Panel A shows data from rats sacrificed at 8 h after AOM administration in the MSC (-) control group of the AARGC model, panel B shows data from rats sacrificed at 8 h after AOM administration in the MSC-24h group, and panel C shows data from AOM-untreated healthy rats. Bar scales at the right lower corner in each panel indicated 10 μm. In panel D, relative expression of *Mgmt* in the mucosa was evaluated by qPCR. *1, $P = 0.021$; *2, $P = 0.018$. Panel E shows the results of western blot analyses of Smad2, phospho-Smad2, IKKβ, IκBα, Bcl-2, Bcl-xL, cIAP-2, p21, Bax, Cdk4, Rb, and phospho-Rb. Lanes 1–5 correspond to 0–24 h, and the left and right panels correspond to the control and MSC-24h groups, respectively. The data are representative of three independent experiments.

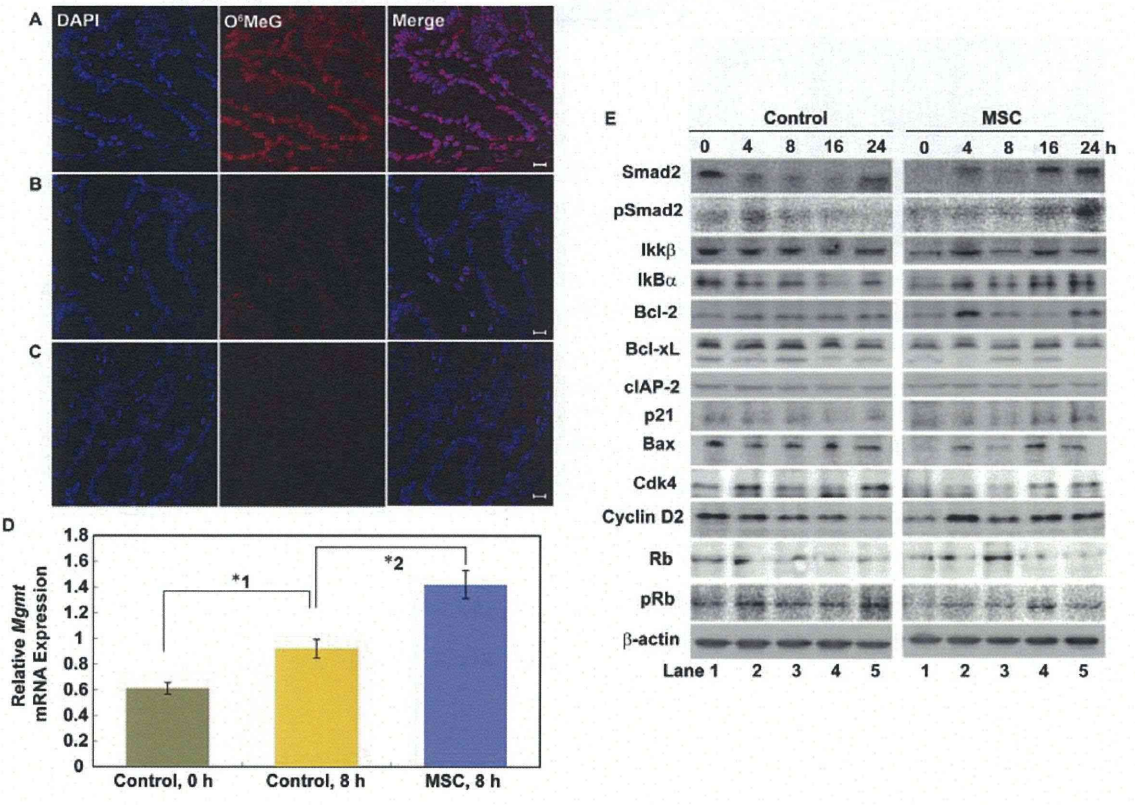

Figure 6. Mechanistic insight into suppression of AOM-induced tumor initiation *in vitro*

The Ki-67 labeling index was calculated in triplicate and bar charts were constructed for the following conditions: IEC-6 cells treated with AOM cocultured with or without MSCs, IEC-6 cells treated with MAM cocultured with or without MSCs, IEC-6 cells treated with AOM and O^6BG cocultured with or without MSCs, and IEC-6 cells treated with MAM and O^6BG cocultured with or without MSC (A). *1, $P = 4.0E-4$; *2, $P = 4.0E-4$; *3, $P = 4.0E-4$; *4, $P = 4.0E-4$; *5, $P = 4.0E-4$; *6, $P = 4.0E-4$; *7, $P = 4.0E-4$; *8, $P = 4.0E-4$; *9, $P = 4.0E-4$; *10, $P = 4.0E-4$; *11, $P = 4.0E-4$. The apoptotic index of IEC-6 cells was calculated based on TUNEL staining in triplicate and bar charts were constructed for the conditions described above (B). Representative Ki-67 immunofluorescence of IEC-6 cells (C) and IEC-6 cell cocultures in which cells emitting green fluorescence are GFP-labeled MSCs (D). Cell culture images were taken at a magnifying power of 630. The cell cycle of cocultured IEC-6 cells was analyzed by flow cytometry at 24 h (left), 48 h (middle), and 72 h (right) in triplicate (E). IEC-6 proliferation was assayed by MTT for the following groups in triplicate: without AOM, cocultured with MSCs (direct), cocultured with MSCs (indirect), treated with MSC-CM, and cocultured directly with MSCs and treated with anti-TGF-β neutralizing antibodies (F).

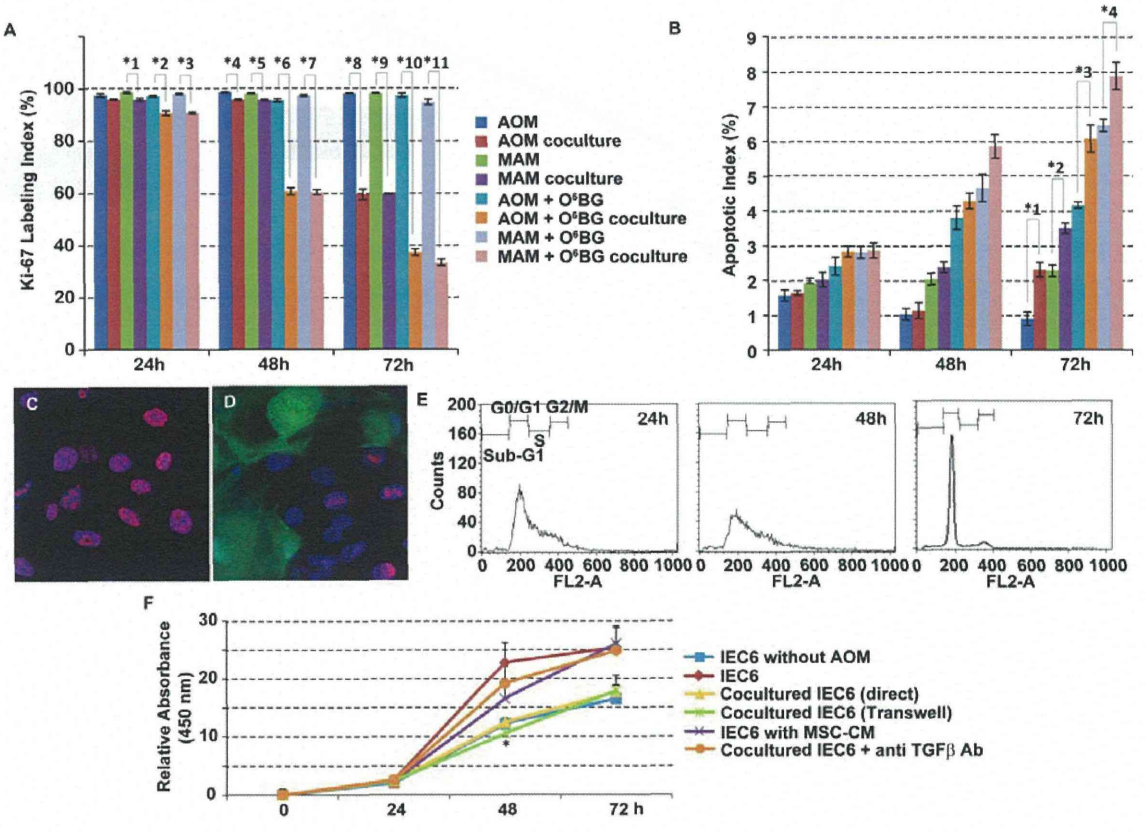

Figure 7. The tandem mechanisms of MSC chemoprevention involved in AOM-induced tumor initiation

The first mechanism of chemoprevention is an indirect measure exerted by MSCs: MSCs activate Mgmt in an unknown manner, resulting in suppression of the AARGC because of a reduction of initiating cells harboring O^6MeG adducts. The second mechanism is a direct measure: MSCs induce G1 arrest in early initiated cells evading the AARGC.

Abbreviations: AOM, azoxymethane; MAM, methylazoxymethanol; O^6MeG, O6-methylguanine.

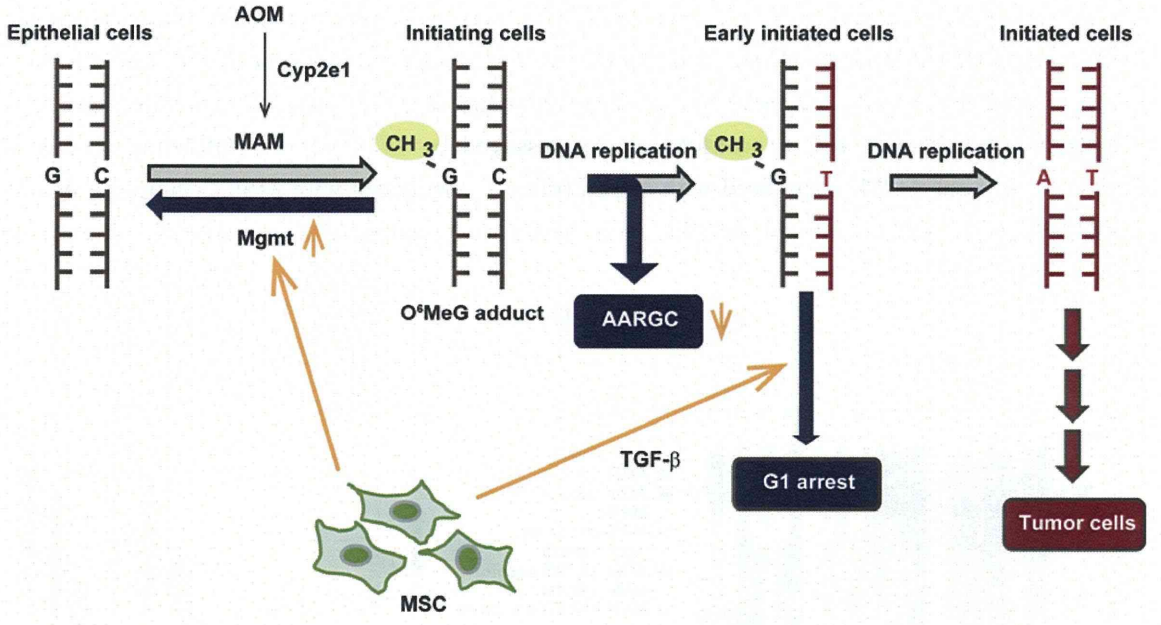

TEB-2013-0578-ver9-Kagami_1P
Type: review-article

TISSUE ENGINEERING: Part B
Volume 00, Number 00, 2014

DOI: 10.1089/ten.teb.2013.0578

AU1 ▶
AU2 ▶

The Use of Bone Marrow Stromal Cells (Bone Marrow-Derived Multipotent Mesenchymal Stromal Cells) for Alveolar Bone Tissue Engineering: Basic Science to Clinical Translation

AU3 ▶ Hideaki Kagami, DDS, PhD,[1–3] Hideki Agata, DDS, PhD,[4] Minoru Inoue, DDS, PhD,[1,2] Izumi Asahina, DDS, PhD,[4] Arinobu Tojo, MD, PhD,[1] Naohide Yamashita, MD, PhD,[2] and Kozo Imai, MD, PhD[5]

Bone tissue engineering is a promising field of regenerative medicine in which cultured cells, scaffolds, and osteogenic inductive signals are used to regenerate bone. Human bone marrow stromal cells (BMSCs) are the most commonly used cell source for bone tissue engineering. Although it is known that cell culture and induction protocols significantly affect the *in vivo* bone forming ability of BMSCs, the responsible factors of clinical outcome are poorly understood. The results from recent studies using human BMSCs have shown that factors such as passage number and length of osteogenic induction significantly affect ectopic bone formation, although such differences hardly affected the alkaline phosphatase activity or gene expression of osteogenic markers. Application of basic fibroblast growth factor helped to maintain the *in vivo* osteogenic ability of BMSCs. Importantly, responsiveness of those factors should be tested under clinical circumstances to improve the bone tissue engineering further. In this review, clinical application of bone tissue engineering was reviewed with putative underlying mechanisms.

Introduction

ATROPHIC ALVEOLAR BONE is one of the major obstacles for dental implant therapy and there are a large number of patients without sufficient bone volume. For patients with severe bone atrophy, autologous bone grafts have been performed.[1] However, even the amount of harvesting bone is small and the procedure is accompanied by swelling and pain of the donor site.[2] Although bioartificial bone substitutes have been frequently used, the ability to induce bone regeneration is limited.[3] Accordingly, less invasive and more efficient bone regeneration therapy is awaited, such as tissue engineering.

The first results of clinical bone tissue engineering were published in 2001.[4] In this study, the regeneration of long bone defects was tested using hydroxyapatite blocks together with cultured autologous bone marrow stromal cells (BMSCs). This tissue engineering-based approach proved the feasibility of this concept. The results from a preliminary clinical study of alveolar bone regeneration were published thereafter.[5] In this review, studies on clinical alveolar bone tissue engineering are summarized. Then, the problems associated with current tissue engineering were also discussed.

Bone Tissue Engineering and Stem Cells

Cells are considered as a major component of tissue engineering. Although the role of transplanted cells during bone tissue regeneration is still controversial, it has been proved that the transplanted cells could survive, proliferate, and differentiate into osteogenic phenotype.[6] There is accumulating evidence that the level and quality of regeneration is affected by the ability of transplanted cells.[7] Accordingly, it is important to establish an optimal cell culture protocol to maximize the function of osteogenic cells. Surprisingly, the BMSC ability to differentiate into osteoblast-like cells is easily diminished during passage and no bone formation was observed after several passages (Fig. 1).[7,8] Furthermore, cell seeding density and the period ◀F1
of induction also affect *in vivo* osteogenic ability. It has been

[1]Tissue Engineering Research Group, Division of Molecular Therapy, The Advanced Clinical Research Center, The Institute of Medical Science, The University of Tokyo, Tokyo, Japan. ◀AU4
[2]Department of Advanced Medical Science, Clinic for Bone Regeneration, IMSUT Hospital, The Institute of Medical Science, The University of Tokyo, Tokyo, Japan.
[3]Department of Oral and Maxillofacial Surgery, Matsumoto Dental University Dental School, Shiojiri, Japan.
[4]Unit of Translational Medicine, Department of Regenerative Oral Surgery, Nagasaki University Graduate School of Biomedical Sciences, Nagasaki, Japan.
[5]Center for Antibody and Vaccine, IMSUT Hospital, The Institute of Medical Science, The University of Tokyo, Tokyo, Japan.

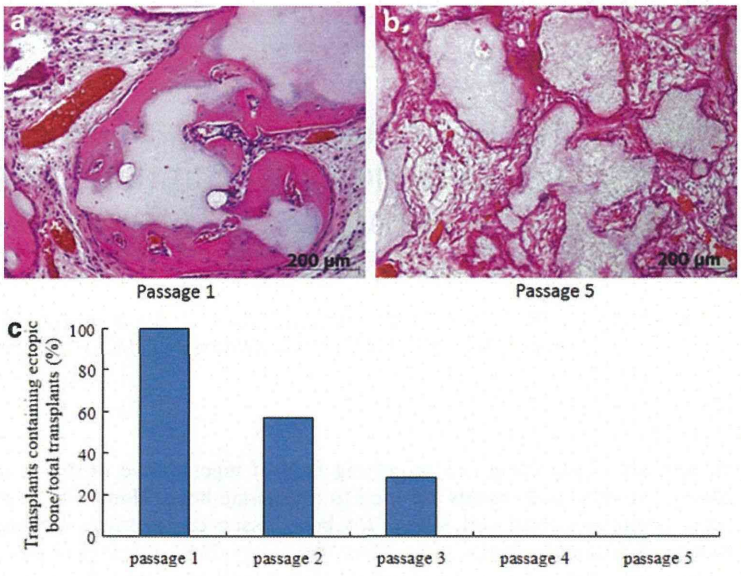

FIG. 1. Effect of passage number on ectopic *in vivo* osteogenic ability. Upper panels showing ectopic bone formation at the back of nude mice with tissue-engineered bone using passage 1 **(a)** and passage 5 **(b)** human bone marrow stromal cells (BMSCs). The success of ectopic bone formation quickly decrease after passage and no bone formation was observed after passage 4 **(c)**. Note that the ability is quickly lost during passage. Modified from Agata *et al.*[7] Color images available online at www.liebert pub.com/teb

shown that basic fibroblast growth factor (bFGF) is beneficial to maintain *in vivo* osteogenic ability of BMSCs.[7]

Clinical Studies on Alveolar Bone Tissue Engineering

The results from clinical studies on alveolar bone tissue engineering using BMSCs were first reported in 2004. In this study, bone marrow-derived MSCs were mixed with platelet-rich plasma as a scaffold.[8] Bone regeneration was observed in all cases. Another clinical study utilized BMSCs and hydroxyapatite granules. BMSCs were induced into osteogenic cells for 1 week and transplanted. In this study, bone formation was observed in three cases, but there was no apparent bone formation from the transplanted cells in

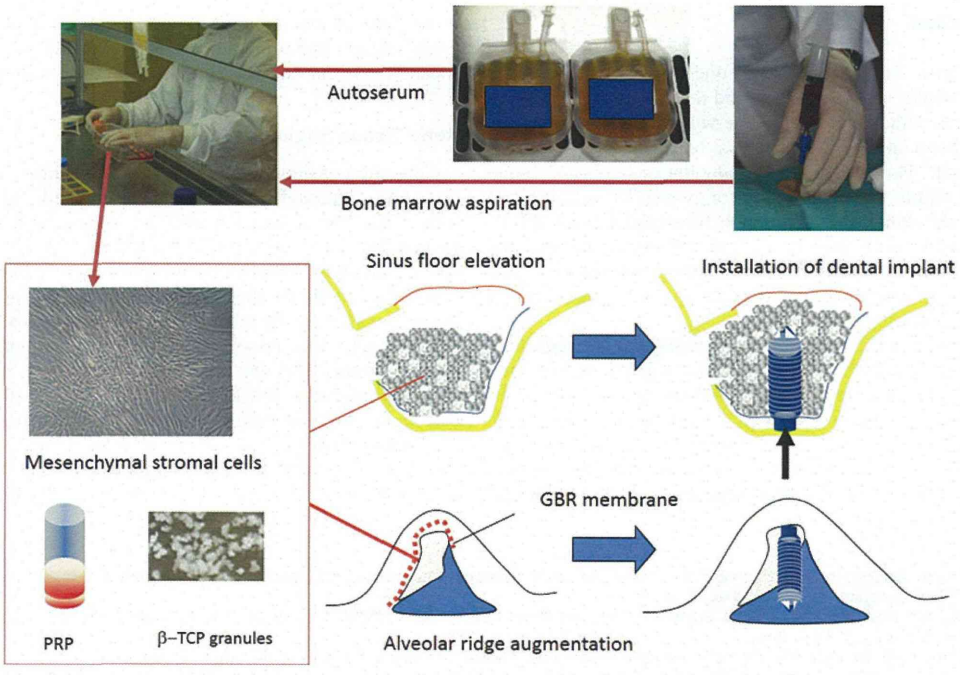

FIG. 2. The procedure for clinical study of alveolar bone regeneration at The Research Hospital, The Institute of Medical Science, The University of Tokyo. β-TCP; PRP. Color images available online at www.liebertpub.com/teb

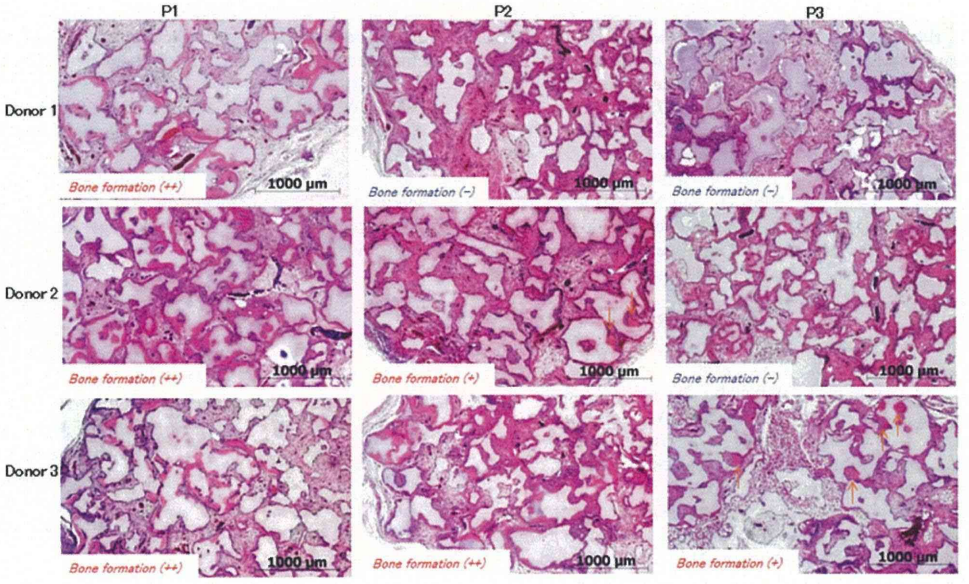

FIG. 3. Individual (donor) variations of *in vivo* osteogenic ability and their changes during passage. Note that the effect of passage differed between individuals. Color images available online at www.liebertpub.com/teb ◀AU8

cases where the atrophy was severe. Thus, the efficacy of clinical alveolar bone tissue engineering for severe atrophy cases remains controversial.

We have conducted a clinical study of bone tissue engineering for severe atrophy of alveolar bone. In this study, autologous BMSCs were transplanted together with platelet-rich plasma gel and β-TCP granules as scaffolds (Fig. 2). F2▶ AU5▶ The results from a 2-year observation showed that bone regeneration was observed in all patients, although significant individual variations in cell growth, differentiation, and levels of bone regeneration were observed (Asahina *et al.*, manuscript in preparation). This type of study, focused on severe atrophy cases, may prove the usefulness of alveolar bone tissue engineering. In terms of safety, no side effects or related complications have been reported, which may imply the relatively safety nature of alveolar bone tissue engineering using BMSCs.

Toward the Establishment of Reliable Alveolar Bone Tissue Engineering Using BMSCs

Although clinical studies have confirmed the feasibility and safety of alveolar bone tissue engineering using BMSCs, one of the important clinical benchmarks is the efficacy for severe atrophy cases. The results from focused studies with selected cases will provide the evidence. Another important problem is the individual variation as shown by basic and preliminary clinical studies. Since the shape and the size of bone defect vary among individuals, it might be impossible to completely eliminate such variations. Accordingly, it should be important to minimize the variation in other factors, such as cells. In terms for BMSCs, there was no significant difference in the expression of mesenchymal stem cell markers during passage.[7] In contrast, a large variation was observed in the *in vivo* bone forming ability among donors and during passage.[7,8] We believe the usage of early passage cells as well as growth factors (bFGF) may minimize the variation, which should be tested under clinical settings.

In spite of the number of studies and the clinical efficacy of bone tissue engineering, it is not a standard treatment at present. It is necessary to show the superiority of clinical outcome compared with standard autologous bone transplantation and allogenic (or xenogenic) transplantation. Furthermore, tissue engineering requires special facility for cell culture and there is a requirement for many safety examinations, which may also increase the cost for treatment. Those technologies, which may support the widespread use of bone tissue engineering, should be investigated.

Tissue engineering is one of the most rapidly progressing fields and alveolar bone is still an attractive target for tissue engineering.[9] The application of bone tissue engineering is not limited for dental implants and is successfully applied for other diseases such as nonunion fractures[10] and alveolar clefts.[11,12]

Disclosure Statement

No competing financial interests exist.

References

1. Jensen, S.S., and Terheyden, H. Bone augmentation procedures in localized defects in the alveolar ridge: clinical results with different bone grafts and bone-substitute materials. Int J Oral Maxillofac Implants **24 Suppl,** 218, 2009.
2. Clavero, J., and Lundgren, S. Ramus or chin grafts for maxillary sinus inlay and local onlay augmentation: comparison of donor site morbidity and complications. Clin Implant Dent Relat Res **5,** 154, 2003.

3. Becker, W., Urist, M., Becker, B.E., Jackson, W., Parry, D.A., Bartold, M., Vincenzzi, G., De Georges, D., and Niederwanger, M. Clinical and histologic observations of sites implanted with intraoral autologous bone grafts or allografts. 15 human case reports. J Periodontol **67,** 1025, 1996.
4. Quatro, R., Mastrogiacomo, M., and Cancedda, R. Repair of large bone defects with the use of autologous bone marrow stromal cells. N Engl J Med **344,** 385, 2001.
5. Yamada, Y., Ueda, M., Hibi, H., and Nagasaka, T. Translational research for injectable tissue-engineered bone regeneration using mesenchymal stem cells and platelet-rich plasma: from basic research to clinical case study. Cell Transplant **13,** 343, 2004.
6. Meijer, G.J., de Bruijn, J.D., Koole, R., and van Blitterswijk, C.A. Cell based bone tissue engineering in jaw defects. Biomaterials **29,** 3053, 2008.
7. Agata, H., Asahina, I., Watanabe, N., Ishii, Y., Kubo, N., Ohshima, S., Yamazaki, M., Tojo, A., and Kagami, H. Characteristic change and loss of *in vivo* osteogenic abilities of human bone marrow stromal cells during passage. Tissue Eng Part A **16,** 663, 2010.
8. Sugiura, F., Kitoh, H., and Ishiguro, N. Osteogenic potential of rat mesenchymal stem cells after several passages. Biochem Biophys Res Commun **316,** 233, 2004.
9. Egusa, H., Sonoyama, W., Nishimura, M., Atsuta, I., and Akiyama, K. Stem cells in dentistry—Part II: clinical applications. J Prosthodont Res **56,** 229, 2012.
10. Shoji, T., Ii, M., Mifune, Y., Matsumoto, T., Kawamoto, A., Kwon, S.M., Kuroda, T., Kuroda, R., Kurosaka, M., and Asahara, T. Local transplantation of human multipotent adipose-derived stem cells accelerates fracture healing via enhanced osteogenesis and angiogenesis. Lab Invest **90,** 637, 2010.
11. Pradel, W., and Lauer, G. Tissue-engineered bone grafts for osteoplasty in patients with cleft alveolus. Ann Anat **194,** 545, 2012.
12. Janssen, N.G., Weijs, W.L., Koole, R., Rosenberg, A.J., and Meijer, G.J. Tissue engineering strategies for alveolar cleft reconstruction: a systematic review of the literature. Clin Oral Investig **18,** 219, 2014.

Address correspondence to:
Hideaki Kagami, DDS, PhD
Tissue Engineering Research Group
Division of Molecular Therapy
The Advanced Clinical Research Center
The Institute of Medical Science
The University of Tokyo
4-6-1 Shirokanedai
Minato-ku
Tokyo 108-8639
Japan

E-mail: kagami@ims.u-tokyo.ac.jp

Received: September 15, 2013
Accepted: January 30, 2014
Online Publication Date:

AUTHOR QUERY FOR TEB-2013-0578-VER9-KAGAMI_1P

AU1: Please note that gene symbols in any article should be formatted as per the gene nomenclature. Thus, please make sure that gene symbols, if any in this article, are italicized.
AU2: Please confirm the correctness of article title.
AU3: Please review all authors' surnames for accurate indexing citations.
AU4: Please confirm the correctness of authors' affiliations.
AU5: Please expand β-TCP.
AU6: "b, The success of ectopic bone" has been changed to "The success of ectopic bone." Please confirm.
AU7: Please define β-TCP and PRP.
AU8: Please cite Fig. 3 in the text.

OPEN ACCESS Freely available online

PLOS ONE

Acquired Deficiency of A20 Results in Rapid Apoptosis, Systemic Inflammation, and Abnormal Hematopoietic Stem Cell Function

Akiko Nagamachi[1☯], Yuichiro Nakata[2☯], Takeshi Ueda[2], Norimasa Yamasaki[2], Yasuhiro Ebihara[3], Kohichiro Tsuji[3], Zen-ichiro Honda[4], Keiyo Takubo[5], Toshio Suda[5], Hideaki Oda[6], Toshiya Inaba[1], Hiroaki Honda[2]*

1 Department of Molecular Oncology, Research Institute of Radiation Biology and Medicine, Hiroshima University, Minami-ku, Hiroshima, Japan, **2** Department of Disease Model, Research Institute of Radiation Biology and Medicine, Hiroshima University, Minami-ku, Hiroshima, Japan, **3** Division of Cellular Therapy, Advanced Clinical Research Center, The Institute of Medical Science, The University of Tokyo, Minato-ku, Tokyo, Japan, **4** Health Care Center and Graduate School of Humanities and Sciences, Institute of Environmental Science for Human Life, Ochanomizu University, Bunkyo-ku, Tokyo, Japan, **5** Department of Cell Differentiation, The Sakaguchi Laboratory of Developmental Biology, Keio University School of Medicine, Shinjuku-ku, Tokyo, Japan, **6** Department of Pathology, Tokyo Women's Medical University, Shinjuku-ku, Tokyo, Japan

Abstract

A20 is a negative regulator of NF-κB, and mutational loss of A20 expression is involved in the pathogenesis of autoimmune diseases and B-cell lymphomas. To clarify the role of A20 in adult hematopoiesis, we generated conditional *A20* knockout mice (*A20*$^{flox/flox}$) and crossed them with *Mx–1Cre* (*MxCre*$^{+}$) and *ERT2Cre* (*ERT2Cre*$^{+}$) transgenic mice in which Cre is inducibly activated by endogenous interferon and exogenous tamoxifen, respectively. *A20*$^{flox/flox}$ *MxCre*$^{+}$ (*A20Mx*) mice spontaneously exhibited myeloid proliferation, B cell apoptosis, and anemia with overproduction of pro-inflammatory cytokines. Bone marrow transplantation demonstrated that these changes were caused by hematopoietic cells. NF-κB was constitutively activated in *A20Mx* hematopoietic stem cells (HSCs), which caused enhanced cell cycle entry and impaired repopulating ability. Tamoxifen stimulation of *A20*$^{flox/flox}$ *ERT2Cre*$^{+}$ (*A20ERT2*) mice induced fulminant apoptosis and subsequent myeloproliferation, lymphocytopenia, and progressive anemia with excessive production of pro-inflammatory cytokines, as observed in *A20Mx* mice. These results demonstrate that A20 plays essential roles in the homeostasis of adult hematopoiesis by preventing apoptosis and inflammation. Our findings provide insights into the mechanism underlying A20 dysfunction and human diseases in which A20 expression is impaired.

Citation: Nagamachi A, Nakata Y, Ueda T, Yamasaki N, Ebihara Y, et al. (2014) Acquired Deficiency of A20 Results in Rapid Apoptosis, Systemic Inflammation, and Abnormal Hematopoietic Stem Cell Function. PLoS ONE 9(1): e87425. doi:10.1371/journal.pone.0087425

Editor: Kevin D. Bunting, Emory University, United States of America

Received August 25, 2013; **Accepted** December 23, 2013; **Published** January 31, 2014

Funding: The authors have no support or funding to report.

Competing Interests: The authors have declared that no competing interests exist.

* E-mail: hhonda@hiroshima-u.ac.jp

☯ These authors equally contributed to this work.

Introduction

NF-κB plays fundamental roles in various physiological and pathological processes, such as immunity, apoptosis, inflammation, and cancer [1,2,3]. In an unstimulated state, NF-κB is sequestered in the cytoplasm by binding to IκB proteins. Upon activation by external stimuli, IκB proteins are phosphorylated by the IκB kinase (IKK) complex and then degraded by ubiquitination. NF-κB is released and translocates to the nucleus where it drives the expression of target genes [1,2,3].

A20, also known as tumor necrosis factor alpha-induced protein 3 (TNFAIP3), now emerges as a major negative regulator of NF-κB signaling [4,5]. A20 comprises an ovarian tumor (OTU) domain at its N-terminus and seven Zn-finger motifs. The OTU domain is predicted to have deubiquitinating protease activity, and the Zn finger motifs possess E3 ubiquitin ligase and ubiquitin-binding activities [4,5]. Thus, A20, acting as a ubiquitin-modifying protein, may participate in a negative feedback loop controlling NF-κB signaling [4,5]. The most compelling evidence that A20 plays an essential role in inhibiting inflammation are results of a gene knockout experiment in which A20 deficient mice prematurely died because of severe systemic inflammation and cachexia [6].

A20 is involved in various human diseases, including hematopoietic malignancies. Frequent loss of A20 expression in B-cell lymphomas caused by biallelic deletions and/or point mutations [7,8] indicates that A20 functions as a tumor suppressor in the hematopoietic system. Moreover, single nucleotide polymorphisms in *A20* are associated with autoimmune and inflammatory diseases, such as systemic lupus erythematosus (SLE) [9,10,11], rheumatoid arthritis (RA) [12,13], and Crohn's disease [14].

An approach to determine whether there is a causative association between A20 mutations and pathogenesis employs mice to target A20 in a tissue-specific manner. A number of A20 conditional knockout (cKO) mice have been generated for this purpose. For example, B cell-specific deletion of *A20* using a *CD19–Cre* transgene results in hyper-responsiveness of B cells and

causes autoimmune disease similar to SLE [15,16,17]. Deletion of A20 from dendritic or myeloid cells using *CD11c–Cre* or *LysM–Cre* transgenes, respectively, also induced autoimmune disease. The former exhibited an SLE-like phenotype [18], and the latter developed an RA-like disease [19]. Moreover, *Villin–Cre* transgenic mice harboring a deletion of A20 from their epithelial intestinal cells showed susceptibility to dextran sodium sulfate-induced colitis [20].

Although these studies provide important insights into the role of A20 as a suppressor of tumorigenesis and autoimmunity, its role(s) in the normal functioning of the hematopoietic system of adults remains to be determined. To address this issue, we created mice in which A20 expression can be inducibly and preferentially ablated in hematopoietic cells.

Materials and Methods

Mice

The detailed procedures for constructing the targeting vector and generating the $A20^{flox/flox}$ mice are described in Text S1 (*A20* cKO mice have been deposited in RIKEN BioResource Center (http://www.brc.riken.jp/inf/en/index.shtml, RBRC05494). $A20^{flox/flox}$ mice were crossed with *Mx–1Cre* ($MxCre^{+}$) transgenic mice [21] and *ERT2Cre* ($ERT2Cre^{+}$) transgenic mice (C57BL/6-Gt(ROSA)26Sor$^{tm1(cre/Est1)Arte}$, purchased from Taconic) to generate $A20^{flox/flox}$ $MxCre^{+}$ and $A20^{flox/flox}$ $ERT2Cre^{+}$ mice, respectively. Mice backcrossed with the C57BL/6-Ly5.2 background at least seven times were used here. This study was carried out in strict accordance with the recommendations in the Guide for the Care and Use of Laboratory Animals of the Hiroshima University Animal Research Committee. The protocol was approved by the Committee on the Ethics of Animal Experiments of the Hiroshima University (Permit Number: A13-13). All mice were maintained according to the guidelines of the Institute of Laboratory Animal Science of Hiroshima University, all surgeries were performed under sodium pentobarbital anesthesia and all efforts were made to minimize suffering.

Western Blotting, Flow Cytometry, and Histopathology

Western blotting, flow cytometry, and histopathology were performed as previously described [22,23,24]. Antibodies and a staining kit used in these analyses are listed in Table S1.

Measurement of Serum Cytokine Concentration

Concentrations of pro-inflammatory cytokines (TNF-α, IFN-γ, GM-CSF, IL-1β, and IL-6) were measured using a BD Cytometric Bead Array Flex Set Kit (BD Biosciences, San Diego, CA, USA) according to the manufacturer's instructions.

Colony Formation Assay

The colony formation assay was performed as previously described [25].

Bone Marrow Transplantation (BMT), Competitive Repopulation, and Cell Cycle Analyses

Transplantation of bone marrow (BM) cells, competitive repopulation, and short-term BrdU incorporation assays were performed as previously described [24].

Results

$A20^{flox/flox}$ $MxCre^{+}$ Mice Exhibited Severe Inflammation, B Lymphocyte Apoptosis, and Premature Death

To conditionally ablate A20 function, we generated mice in which exon 3 of *A20* was flanked by two *loxP* sites ($A20^{flox/flox}$ mice, Fig. S1A and S1B). To examine the role of A20 in hematopoietic homeostasis, we crossed $A20^{flox/flox}$ mice with *Mx–1Cre* transgenic ($MxCre^{+}$) mice in which *Cre* is placed under the control of IFN-responsive *Mx–1* promoter [21]. Lack of A20 expression in $A20^{flox/flox}$ $MxCre^{+}$ mice was confirmed by western blotting of spleen extracts prepared from $A20^{flox/flox}$ $MxCre^{-}$ and $A20^{flox/flox}$ $MxCre^{+}$ mice (hereafter referred to as *control* and *A20Mx* mice, respectively) using an anti-A20 antibody (left panel of Fig. S1C).

Although *A20Mx* mice were apparently normal at birth, they exhibited spontaneous emaciation and cachexia without stimulation by polyinosinic:polycytidylic acid (pIpC), which is a strong and transient inducer of IFN, and most mice died within six months after birth (Fig. 1A). Hematological analysis of moribund mice revealed anemia, proliferation of myeloid cells, and reduction of B lymphoid cells in the peripheral blood (PB) (Table S2). The macroscopic appearance of the mice was uniformly characterized by massive hepatomegaly and enlarged spleens (indicated by an arrowhead and an arrow, respectively, in the left panel of Fig. 1B), which were frequently associated with lymph node (LN) swelling (Table S2). Pathological analysis revealed infiltration of the lung and liver by hematopoietic cells (indicated by arrows in the right top and middle panels of Fig. 1B), formation of granulomas in the liver (indicated by an arrowhead in the right middle panel of Fig. 1B), and destruction of spleen architecture caused by the proliferation of white blood cells (indicated by a white arrowhead in the right bottom panel of Fig. 1B). Higher magnification of the spleen showed that the most of the proliferated cells were with segmented or multi-lobulated nuclei, strongly suggesting that these cells were of myeloid in origin (indicated by arrowheads in the left panel of Fig. S2).

We then analyzed the time-dependent changes in hematopoietic parameters in *control* and *A20Mx* mice. The white blood cell count (WBC), hemoglobin concentration (Hgb), and platelet (Plt) number in the PB, and the absolute numbers of B lymphoid ($B220^{+}$), T lymphoid ($Thy1.2^{+}$), and myeloid ($Mac1^{+}Gr1^{+}$) cells in the PB and spleen were analyzed at three and six months after birth. Although no significant difference was observed in the WBC count and Plt number between the two groups, *A20Mx* mice exhibited progressive anemia (top panels of Fig. 1C). In addition, lineage analysis of WBCs in the PB and spleen revealed that the numbers of myeloid cells were significantly increased, whereas those of B lymphoid cells were significantly decreased in *A20Mx* mice compared with *control* mice (middle and bottom panels of Fig. 1C). To clarify the mechanism of B-cell reduction in *A20Mx* mice, spleens of *A20Mx* mice and control littermates were subjected to and anti-B-cell and TUNEL double staining. As shown in Fig. S3, a significant portion of B lymphocytes in the *A20Mx* spleen was positive for TUNEL, indicating that the B cell reduction in *A20Mx* mice was due to apoptosis.

Because A20 inhibits NF-κB signaling and suppresses inflammatory pathway activity [4,5], we reasoned that the aforementioned findings were caused by sustained inflammatory responses. Therefore, serum concentrations of pro-inflammatory cytokines, including TNF-α, IFN-γ, GM-CSF, IL-1β, and IL-6, were measured and compared between the two groups. The concentrations of these cytokines were higher in *A20Mx* mice than in *control* mice, and those of TNF-α, IFN-γ, and GM-CSF were significantly increased (Fig. 1D). These results indicate that

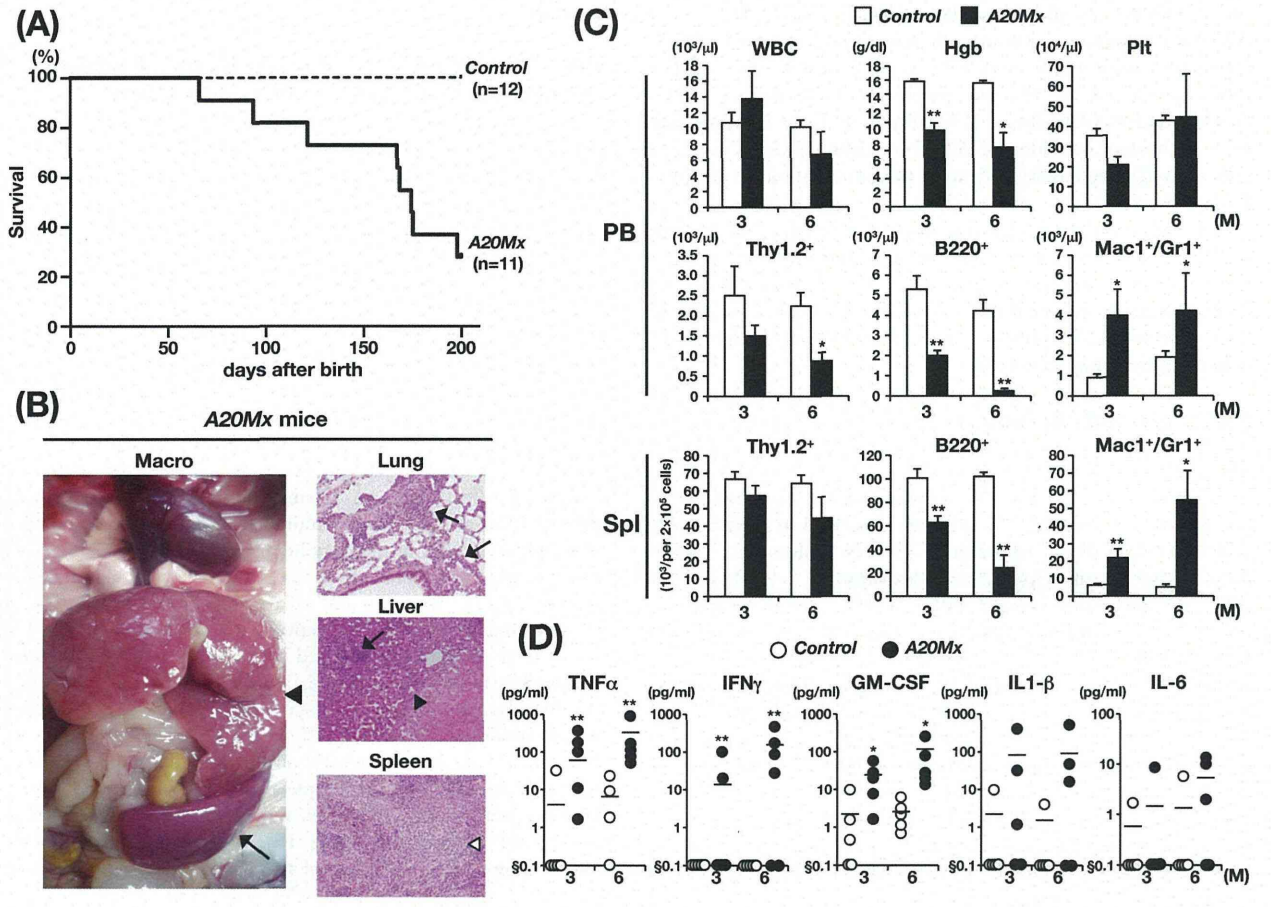

Figure 1. Analysis of *A20Mx* mice. (A) Kaplan–Meier survival curves. (B) Macroscopic appearance and pathological images of an *A20Mx* mouse six months after birth. In the left panel, the enlarged liver and spleen are indicated by an arrowhead and an arrow, respectively. In the right panel, infiltrated myeloid cells in the lung and liver, granuloma formation in the liver, and destruction of spleen architecture are indicated by arrows, an arrowhead, and a white arrowhead, respectively. (C) Time-dependent changes in hematopoietic parameters in the PB and spleen. *p<0.05 and **p<0.01 (Student's *t*-test). (D) Serum concentrations of pro-inflammatory cytokines. *p<0.05 and **p<0.01 (Student's *t*-test). § below standard range and out of invertable range.
doi:10.1371/journal.pone.0087425.g001

cytokine-mediated inflammation induced the proliferation of myeloid cells and other hematopoietic abnormalities, which subsequently damaged internal organs and eventually caused premature death of *A20Mx* mice.

Transfer of the Aberrant *A20Mx* Hematopoietic Phenotype to Naïve Mice

To determine the cellular origin of the severe inflammation observed in *A20Mx* mice, we performed BMT assays. Mononuclear BM cells derived from *control* and *A20Mx* mice were transplanted into lethally irradiated syngeneic recipient mice (hereafter, mice transplanted with *control* and *A20Mx* BM cells are referred to as *control* and *A20Mx* BMT mice, respectively). One month after BMT, all *A20Mx* BMT mice became moribund and were sacrificed to assess hematopoietic and pathological changes. Macroscopically, *A20Mx* BMT mice exhibited thymic atrophy and splenic enlargement (indicated by an arrow and an arrowhead, respectively, in the right top panel of Fig. 2A). Pathological analysis revealed marked infiltration of hematopoietic cells in the lung and liver (right 2nd and 3rd panels of Fig. 2A) and massive proliferation of the same cell types in the spleen (right bottom panel of Fig. 2A) of *A20* BMT mice. The proliferated cells in the spleen were with segmented or multi-lobulated nuclei, indicating that the cells were mature granulocytes, as observed in the *A20Mx* spleen (indicated by arrowheads in the right panel of Fig. S2). Hematopoietic analysis showed an elevated WBC count, reduced Hgb concentration, and decreased Plt number in *A20Mx* BMT mice (top panel of Fig. 2B). Lineage analysis of the PB and spleen revealed a significant increase in the numbers of myeloid cells and a significant decrease in the numbers of B and T lymphoid cells in both tissues (middle and bottom panels of Fig. 2B). The abnormal phenotypes of *A20Mx* BMT mice were similar to those of *A20Mx* mice, indicating that the inflammatory changes detected in *A20Mx* mice were caused by hematopoietic cells.

Impaired Repopulation Ability, Enhanced Cell Cycle Entry, and Constitutive NF-κB Activation in Hematopoietic Stem Cells of *A20Mx* Mice

We then investigated whether the abnormal phenotypes of *A20Mx* and *A20Mx* BMT mice were induced by hematopoietic stem cells (HSCs). HSCs are usually defined as "lineage marker (Lin)$^-$, Sca-1$^+$ and c-Kit$^+$ (LSK)" cells. However, in *A20Mx* mice,

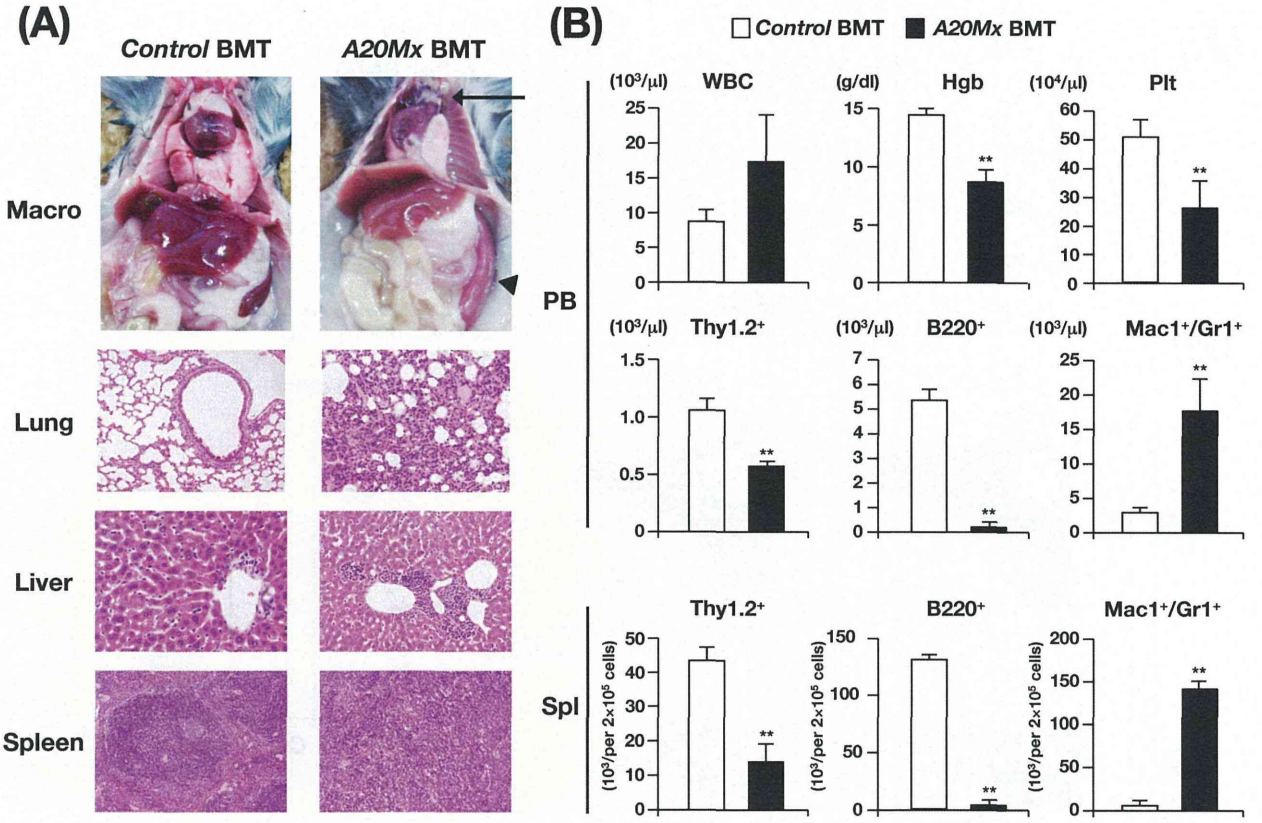

Figure 2. Analysis of *A20Mx* BMT mice. (A) Macroscopic appearance and pathological images of *control* BMT and *A20Mx* BMT mice. The atrophic thymus and enlarged spleen are indicated by an arrow and an arrowhead, respectively. Note the infiltrating hematopoietic cells in the lung and liver and the destruction of spleen architecture caused by excessive proliferation of myeloid cells in *A20Mx* BMT mice. (B) Time-dependent changes in hematopoietic parameters in the PB and spleen. **p<0.01 (Student's *t*-test).
doi:10.1371/journal.pone.0087425.g002

this method is not appropriate, since serum concentration of IFN-γ is elevated and the expression level of Sca-1 was reported to be up-regulated by IFNs [26]. Thus, to isolate HSCs, we used other markers, "Lin$^-$, CD48$^-$, CD150$^+$", called as SLAM-code, which distinguishes HSCs from progenitor cells [27].

HSCs isolated from *control* and *A20Mx* mice (Ly5.2$^+$) were transplanted into lethally irradiated Ly5.1$^+$ recipients together with Ly5.1$^+$ BM MNCs as competitors (hereafter the recipient mice transplanted with *control* and *A20Mx* HSCs are referred to as *control* and *A20Mx* HSC BMT mice, respectively). Interestingly, in contrast that the percentage of Ly5.2$^+$ cells in the PB of *control* HSC BMT mice increased after transplantation and accounted for approximately 40% of WBCs at two months, that of *A20Mx* HSCs BMT mice was significantly less and did not reach 10% of WBCs during the observation period (Fig. 3A). These results indicate severely impaired repopulating ability of HSCs in *A20Mx* mice and suggest abnormal proliferation/differentiation status and cell cycle kinetics of *A20Mx* HSCs.

To address this issue, HSCs isolated from *control* and *A20Mx* mice were subjected to cell counting and short-term 5-bromo-2′-deoxyuridine (BrdU) uptake assay. As shown in Fig. 3B, Although the absolute number of HSCs was considerably decreased in *A20Mx* mice as compared to *control* mice, BrdU uptake by *A20Mx* HSCs was significantly higher than that of *control* HSCs, indicating that *A20Mx* HSCs entered the cell cycle at a higher rate.

A20 is a negative regulator of NF-κB [4,5] and NF-κB activation is detected by its translocation from the cytoplasm to the nucleus [1,28]. To investigate whether NF-κB activation underlies the abnormal behaviors of HSCs, the intracellular localization of NF-κB in HSCs of *control* and *A20Mx* mice were examined by immunofluorescently staining with an anti-NF-κB antibody. In contrast that NF-κB signals in *control* HSCs were mainly observed in the cytoplasm, those in *A20Mx* HSCs were significantly detected in the nucleus (Fig. 3C). These results indicate that NF-κB was constitutively activated in *A20Mx* HSCs, which caused increased cell cycle entry, perturbed their stemness and eventually impaired the repopulating activity.

Rapid Apoptosis and Subsequent Anemia, Myeloid Proliferation, and Reduced Numbers of Lymphocytes Induced by Acquired A20 Deficiency in Hematopoietic Cells

Because the expression of Cre in *MxCre*$^+$ mice was controlled by the IFN-responsive element [21], the activity of Cre was very likely influenced by endogenous IFN. Therefore, we used an *ERT2Cre* transgenic (*ERT2Cre*$^+$) system in which Cre is fused to a mutated estrogen receptor and can only be activated by exogenously administered tamoxifen. For this purpose, we crossed *A20*$^{flox/flox}$ mice with *ERT2Cre*$^+$ mice and generated *A20*$^{flox/flox}$ *ERT2Cre*$^+$ mice (hereafter referred to as *A20ERT2* mice). *A20*$^{flox/flox}$ *ERT2Cre*$^-$ littermates were used as controls. *A20ERT2* mice did

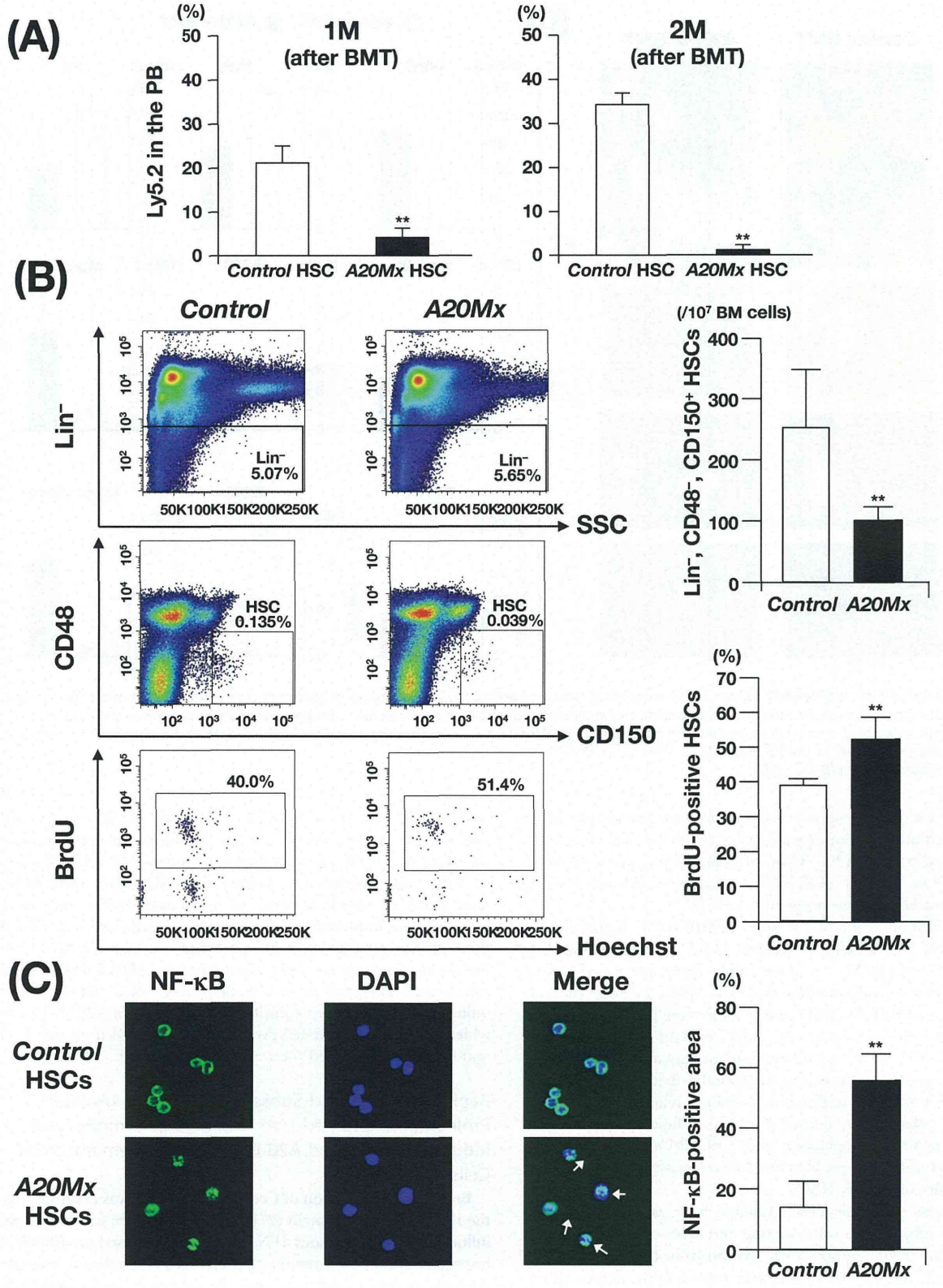

Figure 3. Analysis of HSCs in *control* and *A20Mx* mice. (A) The percentages of Ly5.2$^+$ cells in the PB of *control* and *A20Mx* BMT mice at 1 and 2 months after BMT are shown. **p<0.01 (Student's *t*-test). (B) Cell number and BrdU incorporation in *control* and *A20Mx* HSCs. Representative results of flow cytometry is shown in the left panels and the HSC number and percentage of BrdU-positive cells are shown in the right column. **p<0.01 (Student's *t*-test). (C) Intracellular localization of NF-κB in *control* and *A20Mx* HSCs. Immunofluorescence staining of NF-κB and percentages of the NF-

κB-positive areas in the cells are shown in the left panels and right column, respectively. Cells in which NF-κB is translocated into the nucleus are indicated by arrows. **p<0.01 (Student's *t*-test).
doi:10.1371/journal.pone.0087425.g003

not spontaneously develop abnormal phenotypes in contrast to *A20Mx* mice. However, after tamoxifen administration, *A20ERT2* mice became rapidly moribund, exhibited a marked decrease in the number of hematopoietic cells and died within several days (not shown). Macroscopical examinations revealed that the thymus was atrophic, the spleen was pale, and liver had white spots (not shown). Pathological analysis revealed that massive apoptosis occurred in major organs, including hematopoietic tissues such as the thymus, spleen, liver, and BM (Fig. S4A). Microemboli and necrotic areas were also observed in the liver (indicated by an arrow and arrowheads in Fig. S4A), suggesting that the white spots in the liver were caused by ischemic necrosis. The measurement of pro-inflammatory cytokines revealed that the concentrations of these cytokines were higher in *A20ERT2* mice than in *control* mice, and those of TNF-α, IFN-γ, and IL-6 were significantly increased (Fig. S4B). These results indicate that loss of A20 in adult mice induced fulminant apoptosis, possibly via rapid elevation of pro-inflammatory cytokines.

We next investigated the effect of deleting *A20* from hematopoietic cells by transplanting *control* and *A20ERT2* BM cells into lethally irradiated syngeneic mice and then administrating tamoxifen (mice transplanted with *A20ERT2* BM cells are hereafter referred to as *A20ERT2* BMT mice). Before tamoxifen stimulation, the number of transplanted Ly5.2$^+$ cells was comparably increased in control BMT and *A20ERT2* BMT mice, and there was no significant difference in the values of hematopoietic parameters between them (not shown). Tamoxifen was administered eight weeks after transplantation [29] (Fig. 4A), and two days later, all *A20ERT2* BMT mice became moribund with marked decrease in WBC count and Plt number in the PB ("2 days" at top panels of Fig. 4A).

Tamoxifen-treated *A20ERT2* BMT mice survived this stage, in contrast to *A20ERT2* mice that died after several days after tamoxifen administration, probably because there were no severe apoptotic changes in the non-hematopoietic tissues. Examination of PB parameters showed that *A20ERT2* BMT mice exhibited progressive anemia, proliferation of myeloid cells, and reduction in lymphocyte number, particularly that of B cells, as observed in *A20Mx* and *A20Mx* BMT mice (bottom panels of Fig. 4A). The analysis of the spleen four months after tamoxifen stimulation showed a marked reduction of B and T lymphocytes and a significant increase of myeloid cells (Fig. 4B).

To further investigate whether the changes in the hematopoietic cell population in tamoxifen-treated *A20ERT2* BMT mice were caused by HSCs, competitive repopulation assays were performed. Unlike to the MxCre system, the ERT2Cre system does not respond to endogenous IFNs and no hematological abnormalities were found in the unstimulated state, we used LKS markers to isolate HSCs. LSK cells isolated from control and *A20ERT2* mice were transplanted to the recipient mice and tamoxifen was administered 20 days after transplantation [30]. The recipient mice transplanted with *A20ERT2* LSK cells (hereafter referred to as *A20ERT2* LSK BMT mice, Fig. 5A). While *control* LSK BMT mice were healthy during the observation period, *A20ERT2* LSK BMT mice became gradually emaciated and were sacrificed at 3.5 months after transplantation. The mice showed thymic atrophy and splenomegaly (not shown), and hematopoietic analysis demonstrated anemia and decreased numbers of Ly5.2$^+$ lymphocytes in the PB, elevation of myeloid cell number, and reduction of lymphoid cell numbers in the total and Ly5.2$^+$ fractions of the spleen (Fig. 5A and 5B). These abnormalities were similar to those observed in *A20ERT2* BMT as well as *A20Mx* and *A20Mx* BMT mice. Therefore, we conclude that the abnormalities observed in *A20ERT2* LSK BMT mice can be primarily attributed to the HSCs. Moreover, these abnormalities were found not only in the donor (Ly5.2$^+$) cells but also in the competitor cells (Ly5.1$^+$), indicating that the changes were propagated by cell–cell contact and/or humoral factors, such as pro-inflammatory cytokines.

Discussion

A20 plays an essential role in inflammation, immune system, apoptosis, and tumor suppression [4,5]. The biological roles of A20 in development and in individual tissues have been analyzed using *A20* KO mice [6] and *A20* cKO mice crossed with various Cre transgenic mice [15,16,17,18,19,20,31], respectively. However, to the best of our knowledge, the effect of acquired A20 deficiency on the adult hematopoietic system has not been reported. To address this issue, we generated *A20* cKO mice and crossed them with two different inducible Cre transgenic mice; *Mx1–Cre* and *ERT2Cre* transgenic mice in which Cre is activated in response to endogenous IFN or exogenous tamoxifen, respectively.

A20$^{flox/flox}$ *MxCre*$^+$ (*A20Mx*) mice gradually debilitated and died several months after birth (Fig. 1A) and hematopoietic, pathological, and serological analyses revealed massive inflammatory changes in these mice (Fig. 1B–D). These images of the lung and liver (Fig. 1B), strongly suggest that the mice died of respiratory failure and/or liver dysfunction due to excessive infiltration of hematopoietic cells. Because the *Mx–1* promoter is an IFN-responsive element, it is likely that cells that responded to endogenous IFNs, such as macrophages and lymphocytes, lost the A20 gene, did not attenuate IFN-mediated signaling, and continuously produced pro-inflammatory cytokines, which eventually caused severe systemic inflammation and premature death.

To determine whether the phenotypes of *A20Mx* mice could be primarily attributed to hematopoietic cells, BMT assays were performed. Mice transplanted with *A20Mx* BM cells exhibited abnormal phenotypes similar to those of *A20Mx* mice, indicating that these changes were induced by hematopoietic cells (Fig. 2). We also determined the ability of hematopoietic cells of *control* and *A20Mx* mice to form colonies (Fig. S5). When cultured *in vitro* with SCF+IL3+Epo or SCF+IL7, hematopoietic cells from *control* and *A20Mx* mice formed similar numbers of colonies with similar morphology. Thus, the hematopoietic abnormalities observed in *A20Mx* mice were mainly attributed to excessive production of pro-inflammatory cytokines and systemic inflammation.

To further investigate the effect of A20 deficiency on HSC activity, we performed competitive repopulation assays in which Lin$^-$, CD48$^-$, CD150$^+$ HSCs cells in control or *A20Mx* mice (Ly5.2) were transplanted into recipients with Ly5.1 competitors. Interestingly, the repopulation ability of *A20Mx* HSCs was significantly impaired as compared to that of *control* HSCs (Fig. 3A). In addition, BrdU incorporation assays showed an enhanced proliferative ability of *A20Mx* HSCs (Fig. 3B). Furthermore, NF-κB was activated in a substantial portion of *A20Mx* LT-HSCs as revealed by its presence in the nucleus (Fig. 3C). These results indicated that the loss of A20 in the hematopoietic system activated HSCs, entered them into the cell cycle, and eventually impaired the repopulation ability. Quiescence is an important

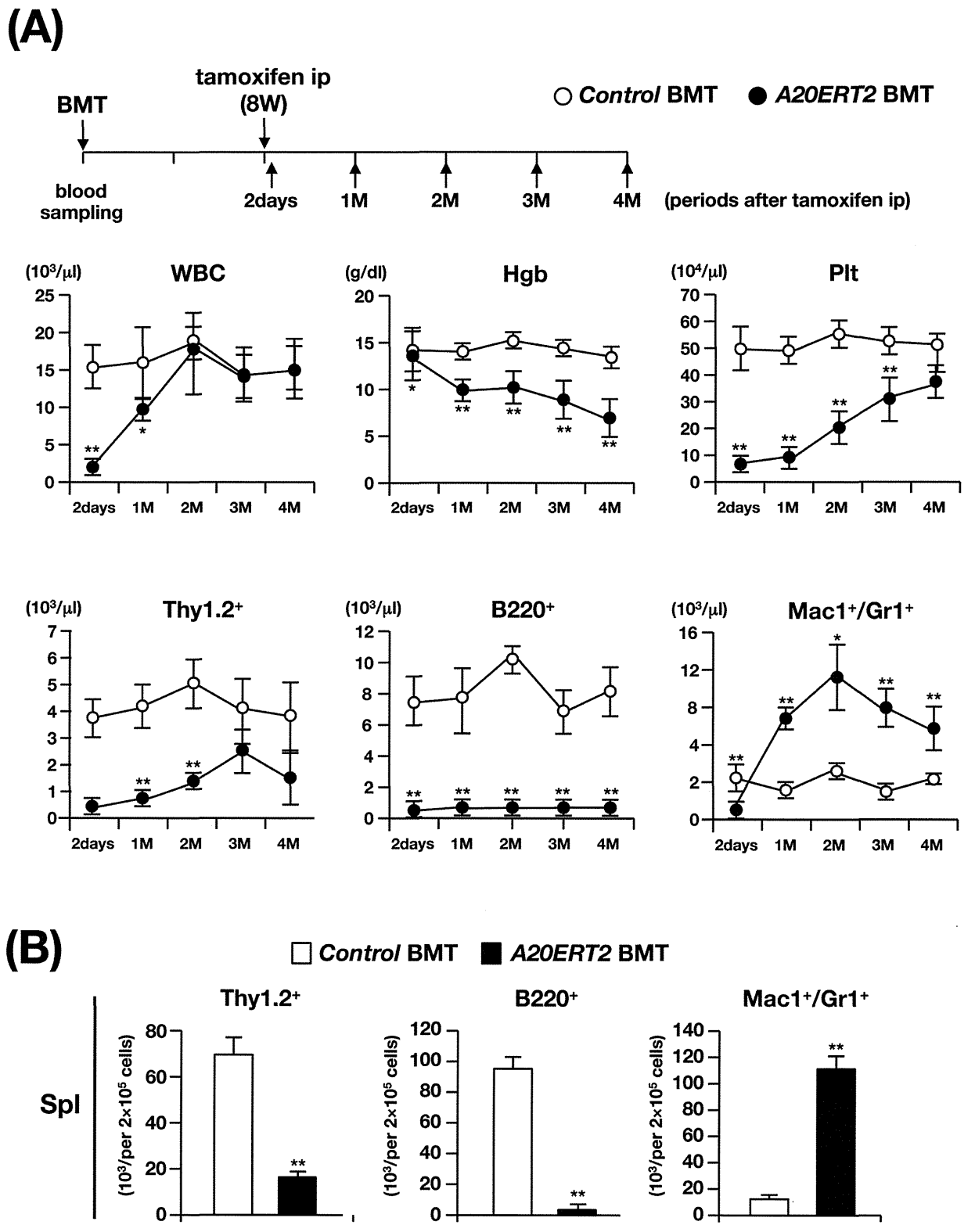

Figure 4. Analysis of *control* and *A20ERT2* BMT mice. (A) Time schedule of BMT, tamoxifen ip, blood sampling, and time-dependent changes in hematopoietic parameters in the PB. **p<0.01 (Student's *t*-test). (B) Percentages of Thy1.2$^+$, B220$^+$, and Mac1$^+$/Gr1$^+$ cells in the spleen 4 M after transplantation. **p<0.01 (Student's *t*-test).
doi:10.1371/journal.pone.0087425.g004